Inácio, Patrick L.; Ferreira, Francisco B.; Vilaça, Pedro; Oliveira, J. P.; Santos, Telmo G.

Assessment of the energetic efficiency of friction stir welding/processing

Published in:
Journal of Manufacturing Processes

DOI:
10.1016/j.jmapro.2023.08.044

Published: 06/10/2023

Document Version
Publisher's PDF, also known as Version of record

Journal of Manufacturing Processes 103 (2023) 298–308

Contents lists available at ScienceDirect

Journal of Manufacturing Processes

journal homepage: www.elsevier.com/locate/manpro

Assessment of the energetic efficiency of friction stir welding/processing

Patrick L. Inácio [a,*], Francisco B. Ferreira [a], Pedro Vilaça [c], J.P. Oliveira [d], Telmo G. Santos [a,b]

[a] UNIDEMI, Department of Mechanical and Industrial Engineering, NOVA School of Science and Technology, Universidade NOVA de Lisboa, 2829-516 Caparica, Portugal
[b] Laboratório Associado de Sistemas Inteligentes, LASI, 4800-058 Guimarães, Portugal
[c] Department of Mechanical Engineering, School of Engineering, Aalto University, 02150 Espoo, Finland
[d] CENIMAT/I3N, Department of Materials Science, NOVA School of Science and Technology, Universidade NOVA de Lisboa, 2829-516 Caparica, Portugal

ARTICLE INFO

Keywords:
Energy
Efficiency
Friction Stir Welding (FSW)
Friction stir Processing (FSP)
Aluminium

ABSTRACT

This paper scrutinizes and goes beyond previously published results on the analysis of the energy flow during friction stir welding/processing (FSW/P). An in-depth scientific method was used to assess the individual energetic contribution arising from the main components within the FSW/P system. This investigation was performed during FSW/P of AA7075 with different tool rotations and travel speeds. The main contributors to energy losses during the FSW/P process include the FSW/P tool, anvil, unprocessed base material, and the surrounding environment. It was found that only about 25 % of the total energy is effectively used to perform the welding/processing, while the remaining energy dissipates through heat into the tooling and clamping system. Additionally, around 6 % of the energy is lost towards the base material, forming the heat-affected zone (HAZ). These results suggest that proper selection of the anvil material offers a promising opportunity to enhance effective energy efficiency, considering that approximately 60 % of the total energy input is lost through this component. Addressing this substantial energy loss becomes essential for achieving a more energetically sustainable industrial application of the FSW/P process.

1. Introduction

Friction Stir Welding (FSW) is a well established solid-state welding process for high quality welds, namely for materials that exhibit poor weldability by fusion-based processes, and dissimilar joints. FSW is an automated and autogenous process which is considered as an environmentally friendly welding solution, since it does not require shielding gases nor emit relevant amounts of hazardous fumes and radiation during operation. Aluminium alloys, such as the AA2XXX and AA7XXX series, Cu- and Ti-based alloys are examples of materials that are often welded by FSW, including some outstanding applications, such as in joining the cover to the 50 mm thick Cu-OFP canisters, that will serve as corrosion protection layer of the spent nuclear fuel [1,2]. Friction Stir Processing (FSP) is similar to FSW but here the objective is to selectively modify the microstructure of the processed materials rather than promoting their joining [3]. For the same materials, the FSW/P peak temperature is significantly lower than in fusion welding [4,5]. But differently from what is frequently claimed in the literature, this fact does not mean less energy input nor high energy efficiency [6].

Eq. (1) presents a breakdown of the mechanical tool energy conversion into two distinct parts: i) Heat energy generated within the material but not consumed in the welded/processed zone, i.e., the energy lost to the surroundings of the welded/processed zone through processes such as conduction, convection, and radiation. ii) Energy that is effectively consumed within the welded/processed zone. This energy facilitates the flow of viscoplastic material and activation of the joining mechanisms. Eq. (2) quantify these energy parcels, were M_z [N·m] is the torque, Ω [rev/min] is the tool rotation speed, F [N] is the transverse force, V [m/s] is the travel speed, t [s] is the welding time, m [kg] is the mass of each FSW/P setup components (e.g. anvil plate, FSW/P tool, welded plates, clamping devices), C_p [J/kg °C] is the specific heat capacity of each component, ΔT [°C] is the difference between the final and starting temperatures of each component.

$$E_{mechanical\ from\ the\ tool} \approx E_{Lost\ elsewhere\ from\ FSW/P} + E_{FSW/P} \tag{1}$$

$$\left(M_z \bullet \frac{2\pi}{60} \bullet \Omega + F \bullet V\right) \bullet t \approx \sum \left(m \bullet C_p \bullet \Delta T\right) + E_{FSW/P} \tag{2}$$

Vilaça et al. showed that during FSW of an AA2024 aluminium alloy, the total mechanical energy per unit of weld length [J/mm] delivered by

* Corresponding author.
E-mail address: p.inacio@campus.fct.unl.pt (P.L. Inácio).

https://doi.org/10.1016/j.jmapro.2023.08.044
Received 5 July 2023; Received in revised form 4 August 2023; Accepted 22 August 2023
Available online 2 September 2023

the FSW tool into the base material outside the TMAZ (thermo-mechanical heat affected zone, including the stirred zone) is less than 10 % [7]. Even within a wide range of parameters encompassing different tool forging forces, F_Z, and weld pitch ratios, Ω/V, the total mechanical energy per unit of weld length was not significantly affected. Thus, over 90 % of energy per unit of weld length is used and then dissipated to the remaining welding system, which includes the tool and tool holder, clamping and anvil plate.

Numerical simulation analysis has been performed by other authors to calculate several process-related features. For instance: Hattel et al. studied the peak temperature of the process and residual stresses developed [8]; Li et al. and Su et al. evaluated the effect of the selected tools on the heat efficiency and material flow [9,10]; Meyghani et al. have developed a finite element model to analyse the thermal aspects of Friction Stir Welding (FSW). They explored various factors, such as the tool tilt angle, to understand their impact on heat generation and material behaviour [11–16]; Cavaliere et al. investigated the crack propagation [17]; Tasić et al. emphasized the significance of considering dwell time during plunging and estimated the heat transfer efficiency and its variation with welding time. Their findings revealed heat transfer efficiencies as low as 5 % for longer welding times [18]. To avoid the complexity of the numerical models, that require multiphysical phenomena and material flow, Vilaça et al. developed an inverse engineering approach, by measuring the real thermal field in the HAZ at both sides of the weld zone, and using an analytical thermal model, to determine the heat power that would generate that thermal field in the far-field domain from the tool [19]. The model encompassed superficial heat losses and features of the 3D asymmetric heat generation during FSW/P. The heat power responsible for the experimentally measured thermal field was determined by an optimization-based iterative algorithm, without need of assumptions on any friction coefficient. This approach enabled reliable assessment of the heat dissipated into the HAZ, but it does not consider the influence of all the components involved in the process, such as tooling, and the anvil plate. Regarding the effect of the anvil plates, there is a significant lack of research of its effect in the process compared to the development of tools for FSW/P.

The demand for sustainable manufacturing processes requires clarification of the effective energy efficiency on the FSW/P processes. The effect of the thermal properties of anvils on FSW/P have been studied by Upadhyay and Reynolds which have set experiments using different anvils materials and forging forces [20,21]. They found that the near root peak temperature and tool torque varied significantly for each case. However, the transfer of the heat energy from the welding/processing zone to the surrounding material/environment must be analysed to determine the effective energy efficiency of the process. That implies analysing not only the conversion of the mechanical energy from the tool to the welding/processing zone, but also consider the energy dissipated into the anvil plate and towards the FSW/P tool. These energy parcels do not contribute directly to the process itself and, as it will be shown, they can represent a high percentage of the overall energy involved during the process.

In this work, we quantify the energy losses during FSW/P for all the components, including the processed material, tool and anvil plate. We show that the effective efficiency of FSW/P is roughly 25 % for aluminium alloys, considering a weld bead with 140 mm length, using an AISI Ck45 steel anvil plate. The description of the energetic parcels for each FSW/P component enables a rational steering of the research towards the energetic efficiency.

2. Process energy efficiency

The overall process energy efficiency was determined by means of an energy balance, assuming that the input mechanical energy is fully transferred from the tool to the welding/processing system, including the FSW/P zone and surroundings, according to the previously described Eq. (1) and Eq. (2).

Fig. 1 illustrates the model of the energy balance. The main goal is to quantify the amount of energy that each component of the FSW/P system dissipates during and after the manufacturing. Some reasonable assumptions were used to simplify the model:

1) The input mechanical energy is completely transferred from the tool to the welding/processing system according to Eq. (1) and as illustrated in Fig. 2;
2) The mechanical energy input regarding the linear movement ($F \bullet V \bullet t$) is neglected, since it is of an order of magnitude lower than the rotation tool energy ($M_z \bullet \frac{2\pi}{60} \bullet \Omega \bullet t$), according to the work of Lambiase et al. [22];
3) Heat losses to the surrounding environment are approximated to zero, owing to the creation of a permanent near adiabatic boundary during the transient heat conduction regime:

- at the anvil side (root side of the welded components), using a Teflon® insulator box;
- at the face side, after completion of FSW/P, the processed Al plate and the top surface of the anvil plate were covered by a 10 mm thick Superwool® 607 HT thermal insulating sheet to emulate an adiabatic boundary.

Fig. 2 depicts the decomposition of the different energy parcels during FSW/P, considering the abovementioned simplifications, i.e. that all mechanical energy input delivered by the FSW/P tool is transferred to the welding/processing zone, and, subsequently, conducted to the tool, Al plate and anvil plate. The remaining energy is considered as consumed in the FSW/P process itself, and its associated to the severe plastic deformation during material stir. Therefore, the FSW/P efficiency can be calculated using Eq. (3), where $E_{FSW/P}$ [kJ] is the FSW/P net energy, E_{IN} [kJ] is the total mechanical energy input and ΣE_{OUT} [kJ] is the total thermal energy output dissipated through the different setup components.

$$\eta_{FSW/P} = \frac{E_{FSW/P}}{E_{IN}} = \frac{E_{IN} - \sum E_{OUT}}{E_{IN}} = 1 - \frac{\sum E_{OUT}}{E_{IN}} \tag{3}$$

3. Materials and methods

A total of nine trials were performed on AA7075-T651 plates with dimensions of 200 × 100 × 5 mm^3 to calculate the effective energetic efficiency during FSW/P (Fig. 3a). AA7075-T651 is a well-known high-strength aluminium alloy widely used for structural components in the aeronautical and automotive industries [23].

Bead-on-plate welding with position control was performed, simulating a FSW/P condition (Fig. 3a). This configuration simplifies the fastening of the Al plate to the anvil plate and does not significantly affect the process parameters nor the energy involved in the tests. A processing length of 140 mm was kept constant for all tests, and the middle point of the bead coincides with the centre of the anvil plate. Trials were performed with different weld pitch ratios, i.e. tool rotation speed to welding speed (Ω/V) ratios. The process parameters presented in.

Table 1 were selected to investigate the impact of welding and tool rotation speeds on the energy efficiency of FSW/P. These choices were based on previous studies conducted by Radisavljevic et al. and Choi et al. In particular, Choi et al. demonstrated that the leading factor influencing energy consumption is the welding speed, although both rotation speed and welding speed contribute to increased power consumption [24,25]. Conducting FSW/P at higher welding speeds leads to a twofold benefit: it enhances productivity and reduces process energy consumption.

A quenched and tempered H13 steel tool (Fig. 3) composed by a concave shoulder with 16 mm in outer diameter and a truncated cone probe, left-hand threaded, and three flutes. The probe was 6 mm in

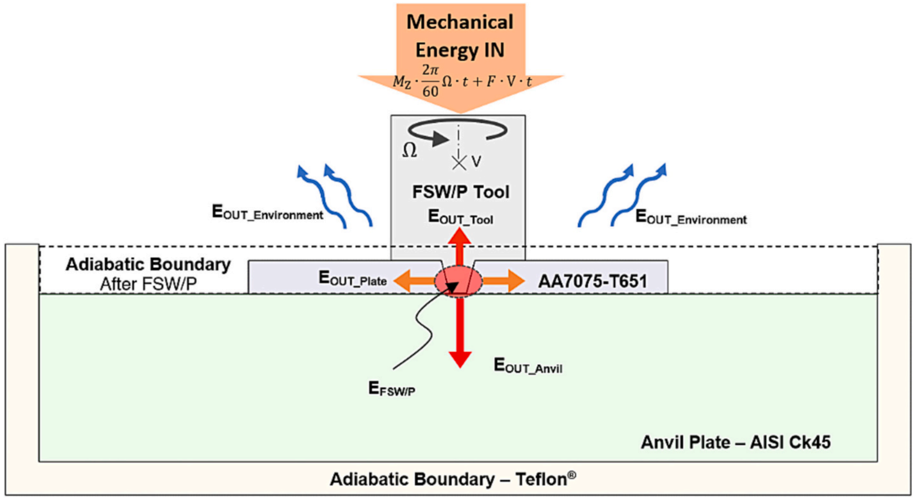

Fig. 1. Schematic of the energy balance of the FSW/P process according to the tested conditions.

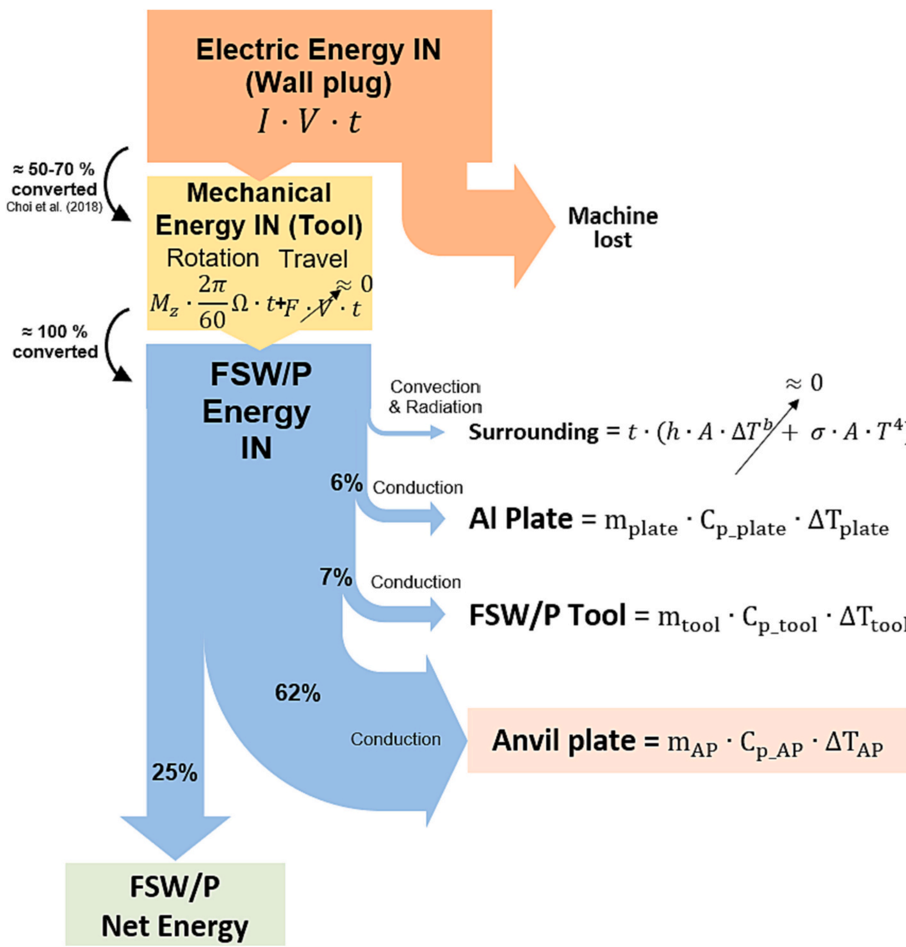

Fig. 2. Illustration of the decomposition of the energy parcels of the FSW/P. The values presented refer to an FSW/P on AA7075-T651 along 140 mm, calculated according to the methodology presented in chapter 3.

diameter at shoulder surface, and 4.8 mm in length. The tool was tilted by 1°.

The anvil plate supports the Al plate with four M8 screws, and it was instrumented with a torque measurement device (refer to Fig. 4) ensuring the simultaneous measurement of the torque applied by the tool. The temperature of the anvil plate was monitored using 23 type K thermocouples (Fig. 5c) to accurately monitor the average temperature evolution during and after the FSW/P. The measurements were performed using a National Instruments NI-9211 Temperature Input Module, integrated within an NI CompactDAQ bundle. This module features a 24-bit ADC resolution and a voltage measurement range of ±80 mV, resulting in a resolution of 9.54 μV. Considering the sensitivity of a K-

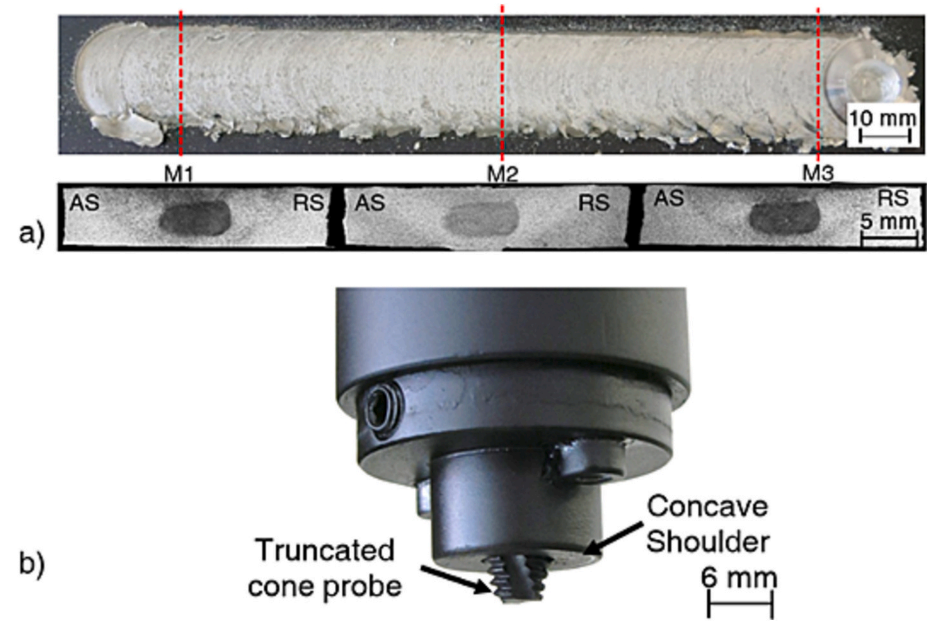

Fig. 3. FSW/P conditions. a) FSW/P bead-on-plate with 140 mm length on a AA7075-T651 plate using a rotation speed Ω = 932 rev/min and a travel speed V = 188 mm/min, b) FSW/P tool with 16 mm concave shoulder and a probe with 6 mm diameter and 4.8 mm length of a truncated cone containing three flutes and LH threads.

Table 1
Processing parameters (Ω and V) of the nine trials performed to compute the FSW/P energy efficiency. Blue: the ratio Ω/V (keeping Ω constant) used to study the effect of travel speed; Green: the ratio Ω/V (keeping V constant) used to study the effect of rotation speed.

		V [mm/min]					
		101	131	188	246	311	373
Ω [rev/min]	588	Ω/V=5.8	4.5	**3.1**	2.4	1.9	1.6
	763	7.6	5.8	**4.1**	3.1	2.5	2.0
	932	**9.3**	**7.1**	**5.0**	**3.8**	**3.0**	**2.5**
	1214	12.1	9.2	**6.5**	4.9	3.9	3.3

type thermocouple, which is approximately 41 μV/°C, the temperature measurement resolution using these thermocouples with the ADC is approximately 0.232 °C. To make the computation of the input energy more accurate the spindle rotation speed, the electrical voltage and current at the terminals of the spindle motor were also acquired. The temperature profile of the tool and the temperature of the top surface of the Al plate (Fig. 5b) were also monitored and recorded during all tests by an infrared thermography camera Fluke® Ti400, with a temperature measurement range of −20 °C to 1200 °C, a Noise Equivalent Temperature Difference (NETD) of 50 mK, in the spectrum 7.5–14 μm, an accuracy of ±2 °C and spatial resolution (iFOV) of 2.62 mRad.

Table 2 depict the physical and thermal properties of the component's materials used during FSW/P considered in the process efficiency analysis.

4. Results and discussion

4.1. Energy delivered by the FSW/P tool

Fig. 6 depicts the typical torque evolution over time for the produced bead-on-plate welds. According to [28,29], the process can be divided in four stages:

I) plunge time – time elapsed during tool insertion until the plunge depth is attained, coincident with the shoulder contacting the face side of the processed base materials;
II) dwell time – time to increase towards stabilization of the tool and workpiece temperature;
III) FSW/P time – time to perform the welding/processing along the processing line;
IV) retraction time – time necessary to complete removal of the tool.

During the plunge time, there is an increase in torque and mechanical power when both the FSW/P tool probe and shoulder contact the material. In stage II (dwell time), torque decreases as the tool and workpiece temperature rises, softening the processed material. When the traverse movement starts in stage III, torque increases initially due to a transient regime, followed by a stationary regime with a minor torque decrease as the material temperature ahead of the tool rises. However, it is important to note that these trials were conducted over a relatively short length (140 mm). For higher travel speeds, the welding time decreases, leading to a reduced contribution of the stationary regime to the total mechanical energy input.

The mechanical power input delivered by the FSW/P tool can be calculated in good approximation, according to Eq. (4), where M_z [N·m] is the torque and Ω [rev/min] is the tool rotation speed. Thus, the total mechanical energy input may be calculated by the time integral of the mechanical power input curve.

$$Power = M_z \bullet \frac{2\pi}{60} \bullet \Omega \text{ [W]} \quad 4$$

Fig. 7 represents the relationship between total mechanical energy input, average mechanical power input, and average torque over the 140 mm processed length for different travel speeds (with constant tool rotation at Ω = 932 rev/min). It can be observed that, the total mechanical energy input decreases significantly with increasing travel speed, while mechanical power slightly increases. Additionally, the average torque demonstrates an increasing trend as the travel speed increases. In Fig. 8, we explore the effect of changing the tool rotation speed, Ω, while keeping the travel speed constant (V = 188 mm/min). In this case, both average mechanical power input and mechanical energy input remain constant, irrespective of the tool rotation speed. This

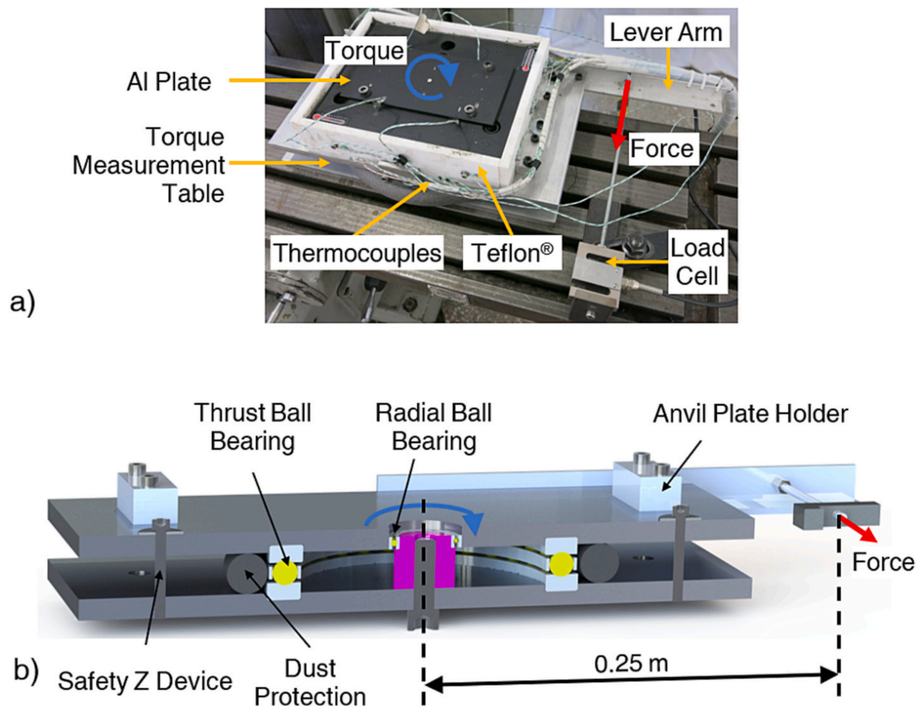

Fig. 4. Instrumented setup for the experimental FSW/P tests. a) Overview, b) Schematic cross-section of the torque measurement device.

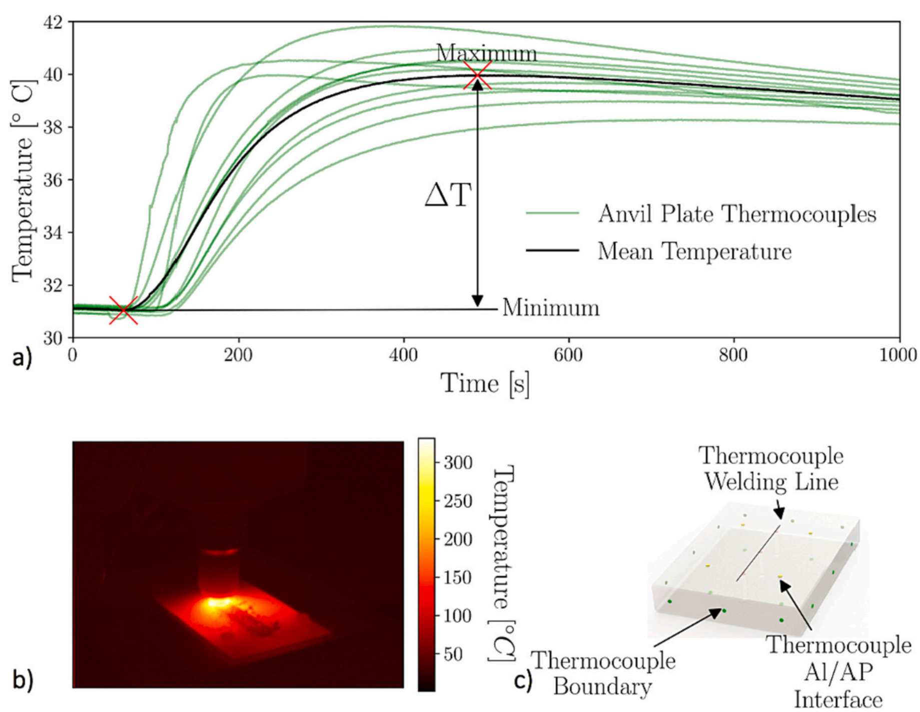

Fig. 5. Measurement of the thermal field during FSW/P. a) Temperature evolution over time for the different thermocouple positions on the anvil plate, b) Temperature distribution on FSW/P tool and processed material, c) Positioning of the 23 thermocouples in the anvil plate (AP).

observation can be explained by the inverse relationship between average torque and tool rotation speed.

Using a linear regression, the total mechanical energy input over the 140 mm processed length, delivered by the FSW/P tool, E_{In} [kJ], can be correlated with the travel speed, V [mm/min], according to Eq. (5), where the tool rotation speed was set as $\Omega = 932$ rev/min. The torque, M_z [N·m], can be correlated with the rotation speed, Ω [rev/min], according to equation Eq. (6), where the travel speed was set as $V = 188$ mm/min.

$$E_{IN} = -0.38 \bullet V + 220 \ (with\ R^2 = 0.89) \tag{5}$$

$$M_z = -0.02 \bullet \Omega + 45 \ (with\ R^2 = 0.99) \tag{6}$$

Table 2
Physical and thermal properties of the FSW/P components [26,27].

FSW/P component	Material	Mass [kg]	Cp [J/kg·°C]	Thermal diffusivity [m^2/s]
FSW/P tool	H13 Steel	0.58	519	6.01×10^{-6}
Al plate	AA7075-T651	0.28	900	5.14×10^{-5}
Anvil plate	AISI Ck45	13.77	522	1.21×10^{-5}

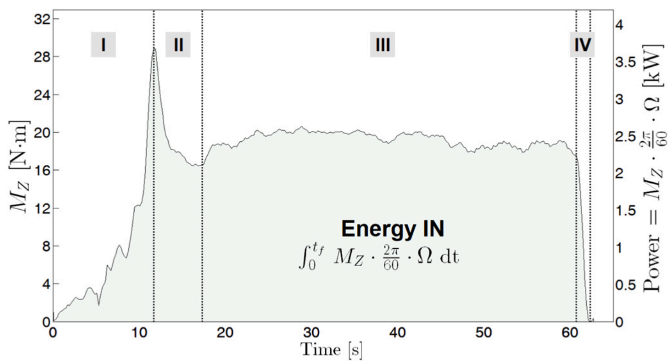

Fig. 6. Torque history over the time for a 140 mm length FSW/P on the AA7075-T651 plate, with thickness of 5 mm, using a rotation speed $\Omega = 1214$ rev/min, and a travel speed $V = 188$ mm/min. Legend: I) plunge time; II) dwell time; III) welding time; IV) retraction time.

4.2. Energy dissipated (E_{OUT}) through the components

The temperature of the instrumented anvil plate was measured before, during and after the FSW/P trials. The final homogenous temperature of the anvil plate was established based on the maximum value of the mean temperature of the 23 thermocouples (refer to Fig. 5c). This criterion considers that a certain period is needed to uniformize the temperature of the anvil plate, after which the global temperature starts to decrease due to the heat flow through the non-perfect adiabatic boundary.

Fig. 9 depicts the temperature increase at the anvil plate, tool and Al plate after the FSW/P. When the travel speed increases, there is a reduction of temperature, as a result of reduced interaction time between the tool and the material. For a constant travel speed, the tool rotation has a small effect in temperature evolution of the components, since the mechanical power is nearly constant.

Fig. 10 depicts the heat energy lost via conduction to the anvil plate, tool and Al plate after FSW/P. These values were calculated using the fundamental equation of calorimetry, that is one of the terms of the Eq. (2). The heat energy conducted from the processed zone into the remaining part of the Al plate quickly transfers to the anvil plate through conduction, primarily due to the anvil plate's higher thermal diffusivity (5.14×10^{-5} m^2/s). Despite a significant increase in temperature, the energy dissipated by the FSW/P tool remains low due to its reduced mass (0.58 kg). On the other hand, the energy dissipated through the anvil plate is the most substantial among all components, and it correlates with the travel speed V [mm/min], when $\Omega = 932$ rev/min, according to Eq. (8).

$$E_{OUT\ Anvil\ plate} = -0.22 \bullet V + 134 \left(with\ R^2 = 0.91 \right) \tag{8}$$

4.3. Overall energy balance of FSW/P

Fig. 11 depicts the total mechanical energy input and the sum of all heat losses during FSW/P. The energy difference between these (E_{IN}-E_{OUT}) can be considered as the energy effectively used to weld or process the material, according to Eq. (2).

After identification and characterization of the dissipated energy parcels across the different components of the FSW/P equipment, the effective energetic efficiency of the process can be calculated.

Considering the travel speed variation (refer to Fig. 12), there is no tendency on the absolute value of the FSW/P energy observed, regarding the process efficiency, which was calculated according to Eq. (4). Overall, the effective energy efficiency during FSW/P of this AA7075 plate was approximately 25 %. This result suggests that FSW/P efficiency is almost independent of the travel speed (V). Similarly, the FSW/P efficiency for different rotation speeds, Ω, was also around 25 %, displaying minimal impact on the overall FSW/P efficiency. Taking all experiments into account, the average efficiency during FSW/P of this AA7075 plate is 25.1 ± 2.9 %.

Fig. 13 provides a comprehensive summary of the energy dissipation through each component of the FSW/P setup. Notably, the anvil plate has the most significant impact on energy consumption/dissipation, playing a crucial role in determining the process efficiency. In total, approximately 62 % of the input energy is dissipated through this component. In an industrial setting, these losses could be even more substantial, considering larger dimensions and weight of anvil plates.

These findings support the importance of carefully selecting the anvil plate material and its initial condition before conducting FSW/P. Since the heat energy in FSW/P mainly arises from friction dissipation in the bulk viscoplastic material flow, the peak temperature is limited by the

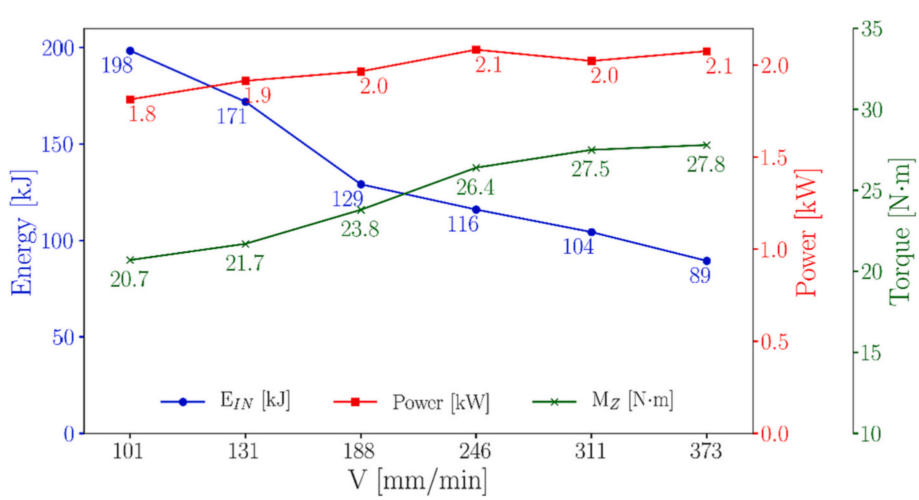

Fig. 7. Total mechanical energy input over the 140 mm processed length, average mechanical power input and average torque for different travel speed, keeping $\Omega = 932$ rev/min.

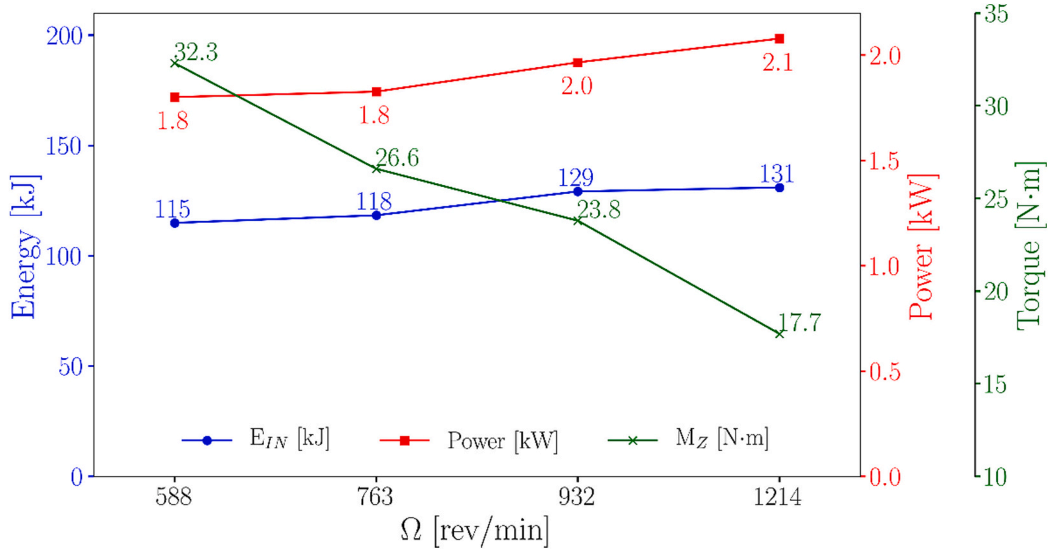

Fig. 8. Total mechanical energy input over the 140 mm processed length, average mechanical power input and average torque for different tool rotation speed, keeping V = 188 mm/min.

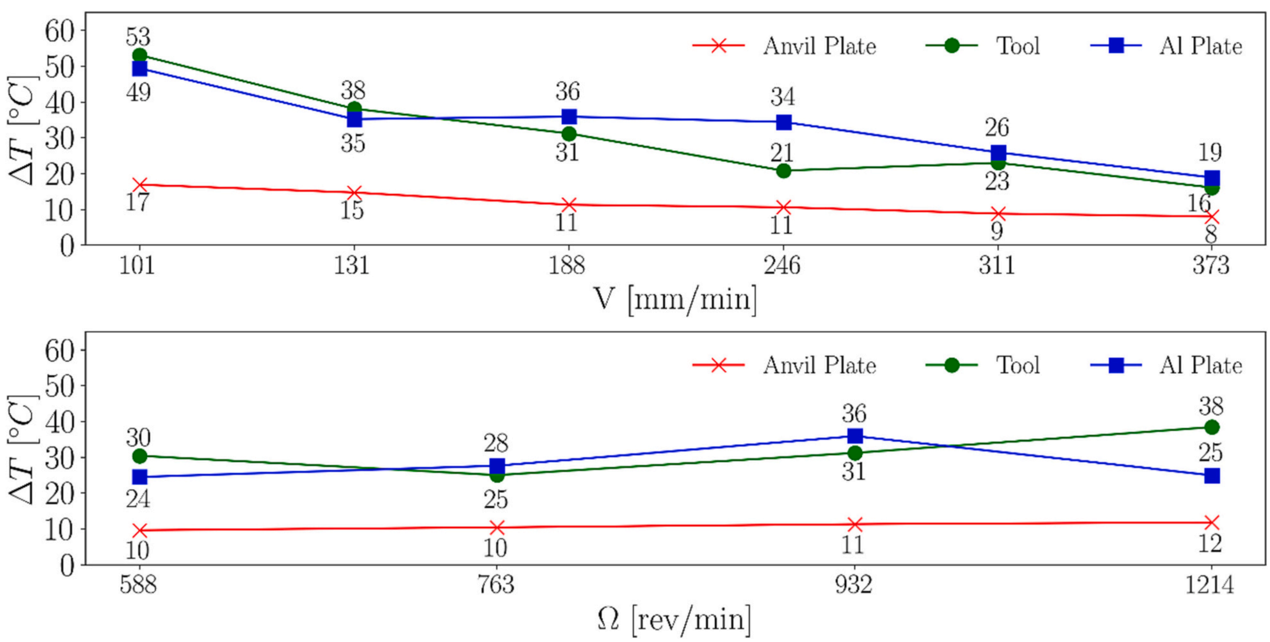

Fig. 9. Temperature increase at the anvil plate, tool and Al plate after the FSW/P: a) effect of travel speed keeping Ω = 932 rev/min; b) effect of tool rotation speed keeping V = 188 mm/min.

material strength and physical properties in the processing temperature domain. However, the size and temperature history of the heat-affected zone (HAZ) heavily depend on how heat flows away from the processed materials.

Therefore, an anvil system with high energy extraction capacity from the Al plate results in a smaller HAZ size and lower energy efficiency in the FSW/P process. Conversely, an anvil that insulates the heat energy within the Al plates leads to higher FSW/P energetic efficiency but may cause a larger HAZ with an overall hotter temperature history. Depending on the Al plates composition and original microstructure, this could potentially result in some level of overaging and softening of the HAZ. Hence, the selection of the anvil plate plays a critical role in achieving optimal energy efficiency and desired weld characteristics in FSW/P applications.

The FSW/P tool is a crucial component in this process, and efforts have been made by the scientific community to develop and optimize new tools, as reported by Rabby and Reynolds [30]. However, the impact of the tool on energy loss was found to be marginal, accounting for approximately 7 % of the total input energy. Nonetheless, the thermal boundary condition used in this study for FSW/P was not fully adiabatic, leading to some energy loss from the FSW/P tool to the machine, which was not measured. If measured, this could have resulted in a slight decrease in process efficiency.

This comprehensive assessment of the energy efficiency associated with FSW/P of the AA7075 plate offers valuable insights to the welding community, providing clear indications on how to develop new solutions for improving the overall process energy efficiency.

Previously, Vilaça et al. (2007) [7] investigated the energy dissipation forming the heat-affected zone (HAZ) and found that only about 5 % of the mechanical power was utilized in producing the HAZ in

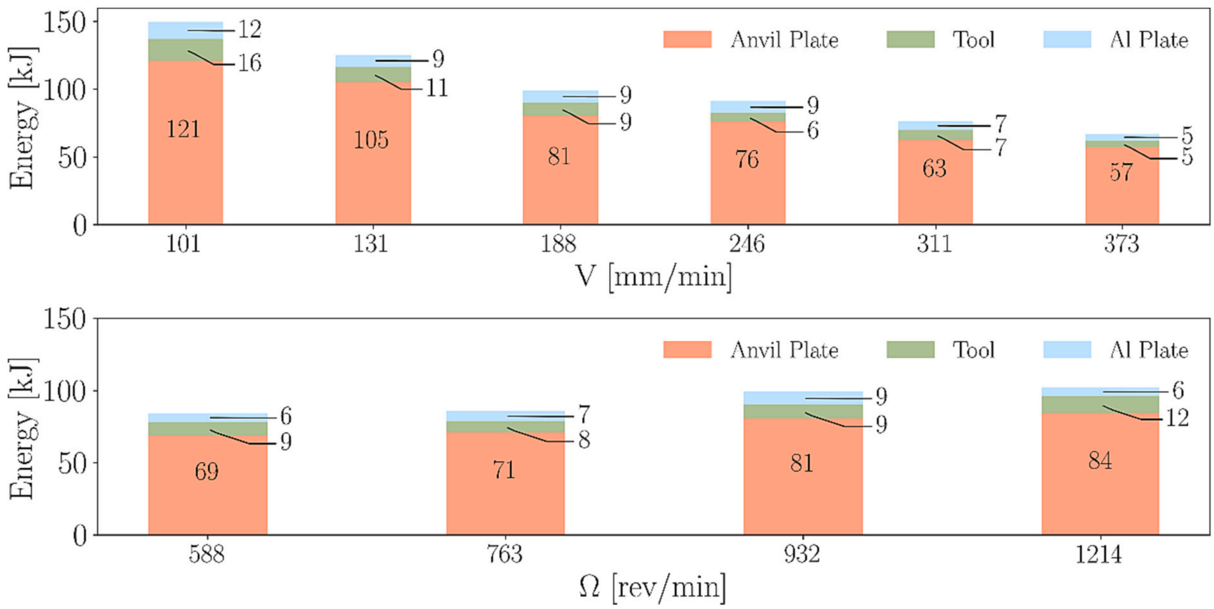

Fig. 10. Heat energy lost via conduction to the anvil plate, tool and Al plate after the FSW/P: a) effect of travel speed keeping Ω = 932 rev/min; b) effect of tool rotation speed keeping V = 188 mm/min.

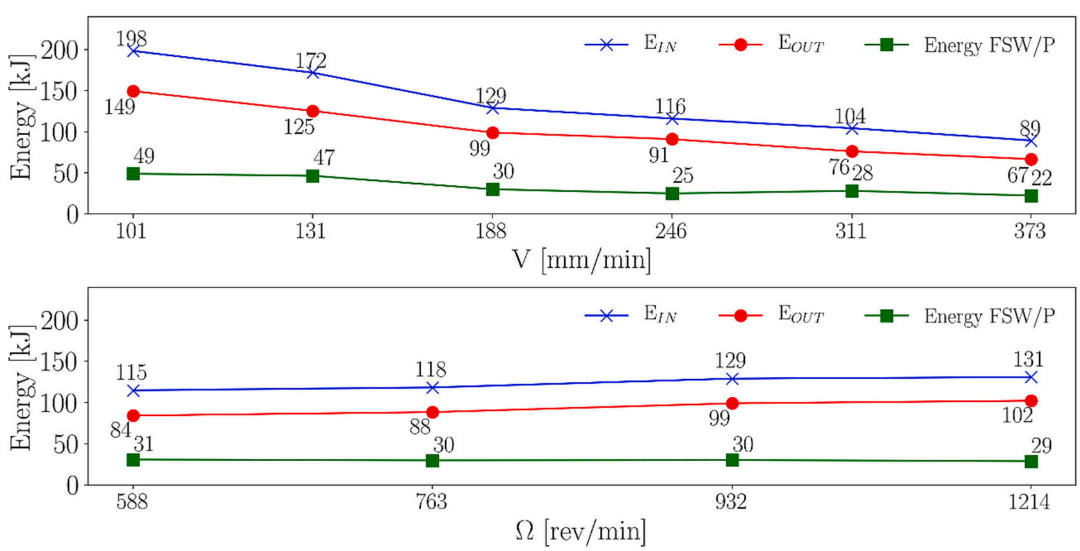

Fig. 11. Comparison between total mechanical energy input ($M_Z \bullet \frac{2\pi}{60} \Omega \bullet t$) and total thermal energy output $\Sigma(m_i \cdot c_p \cdot \Delta T_i)$ for: a) effect of travel speed keeping Ω = 932 rev/min; b) effect of tool rotation speed keeping V = 188 mm/min.

aluminium alloys. The results in the present investigation are fully in line with that finding and clarifies that the remaining 95 % is far from being the process efficiency, when considering the remaining energy losses into the anvil and tool.

The FSW/P efficiency was not significantly affected by the tool rotation speed and travel speed, emphasizing that the approximately 25 % of FSW/P efficiency is an inherent characteristic of the process rather than a result of specific parameters. This implies that about 75 % of the energy is not utilized in producing the thermomechanical processed zone, such as the joint, which opens-up significant opportunities for innovation in this field.

It must be highlighted that the energy dissipation through each component of the FSW/P setup is regarding the transient regime of the process. In fact, after a long period of time, all energy will be dissipated into the surrounding environment, and only the energy parcel associated with the FSW/P process itself (about 25 %) will remain in the welding bead in the form of plastic deformation. Fig. 14 depicts the evolution of the different energy parcels over time.

5. Conclusions

The effective energetic efficiency of the FSW/P was quantified and the contribution from each component of the FSW/P setup determined. The influence of the travel speed and tool rotation speed on the energy balance was established, as these parameters play a crucial role in the FSW/P process. This study provides valuable insights into the energy efficiency of the FSW/P process for AA7075 plate welding.

- It was found that approximately 25 % ± 2.9 %. of the input energy is effectively utilized for the FSW/P process, while the remaining 75 % is lost through various components, with the anvil plate being the most significant contributor to energy dissipation.

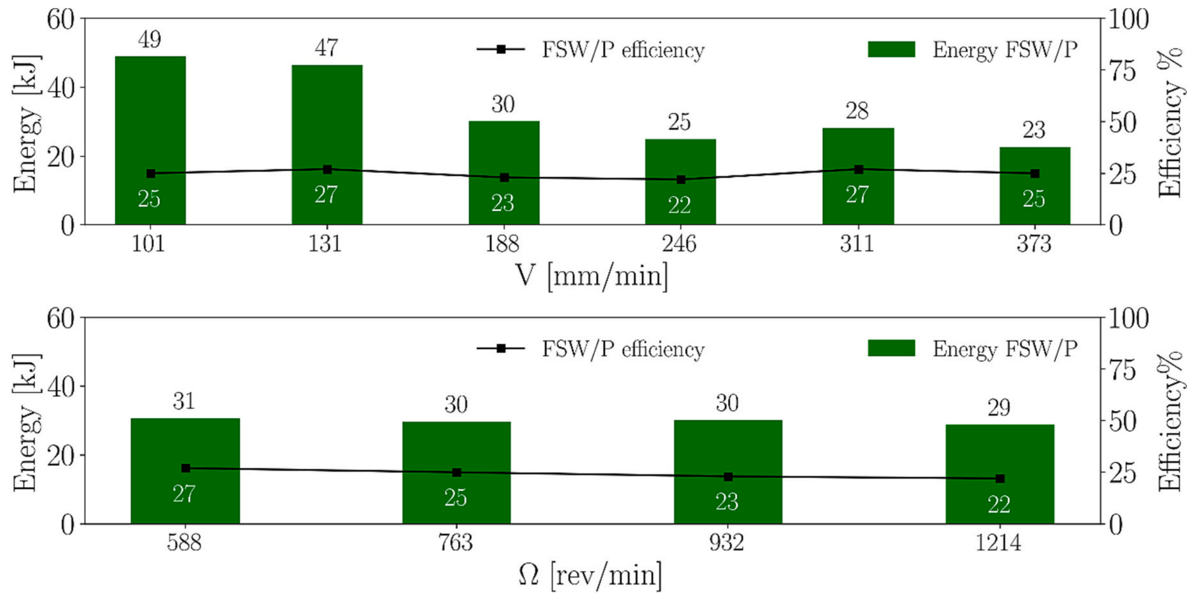

Fig. 12. Energy and efficiency of the FSW/P of the AA7075 plate: a) effect of travel speed keeping Ω = 932 rev/min; b) effect of tool rotation speed keeping V = 188 mm/min.

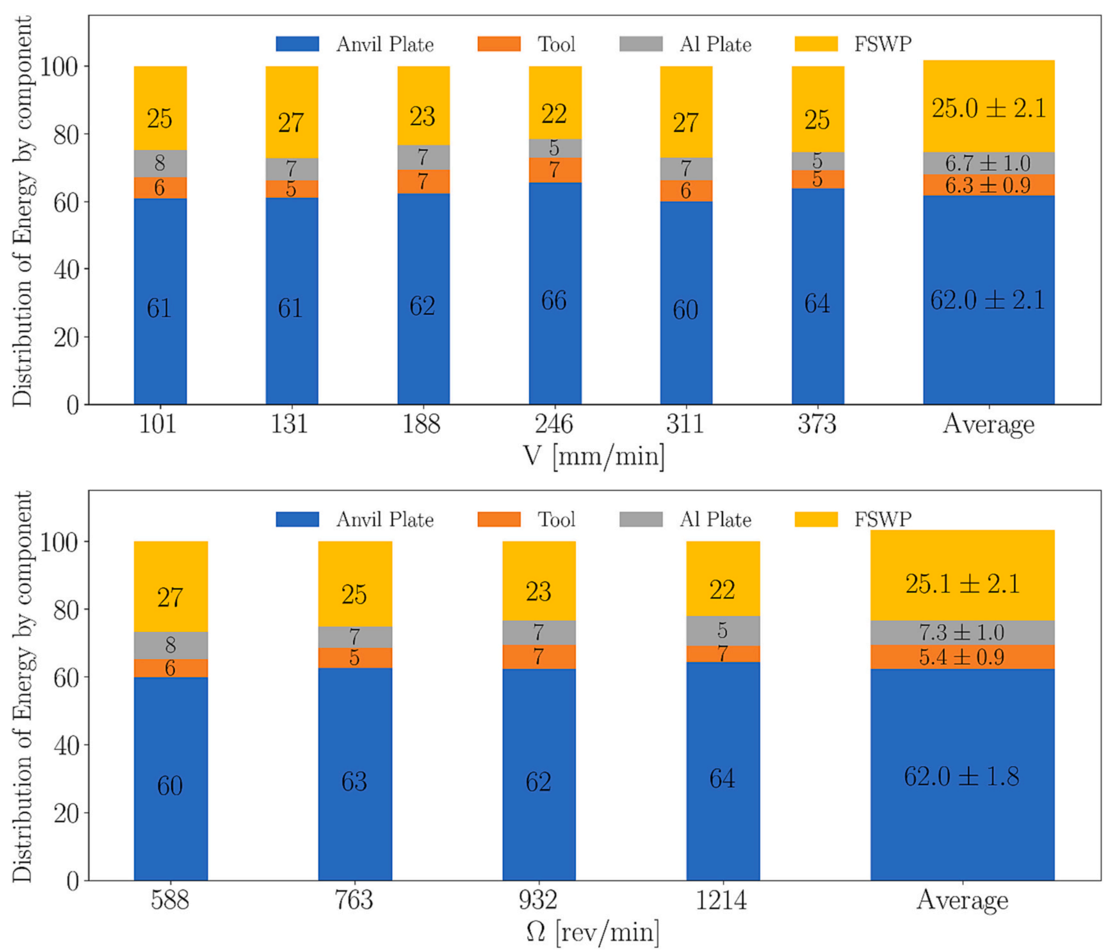

Fig. 13. Energy dissipated through each component of the FSW/P setup: a) effect of travel speed keeping Ω = 932 rev/min; b) effect of tool rotation speed keeping V = 188 mm/min.

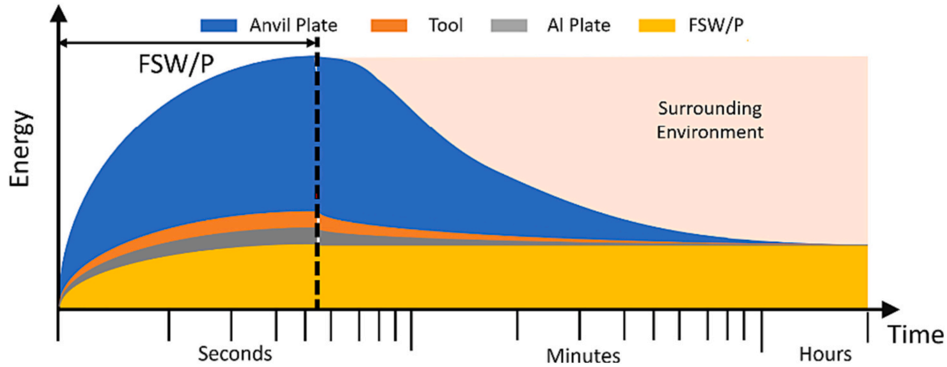

Fig. 14. Schematic illustration of the evolution of the different energy parcels of FSW/P over time.

- For the FSW/P conditions tested, the total energy input for the 140 mm length weld was 189 kJ and 89 kJ, for the lowest (101 mm/min) and highest (373 mm/min) travel speeds, respectively. Across trials with different tool rotation speeds, the average total energy input remained consistent at approximately 123 kJ, with a standard deviation of ±5 %.
- Despite the significant effect of process parameters on the temperature variation of each component, the FSW/P efficiency remains relatively consistent across different tool rotation speeds and travel speeds, indicating that it is an inherent characteristic of the process rather than a parameter-dependent outcome. These findings open up exciting opportunities for innovation and further research in enhancing the overall energy efficiency of FSW/P applications.
- Most of the energy, approximately 62 % of the FSW/P total energy input, is absorbed by the anvil plate. This highlights the anvil plate crucial role in controlling losses in the manufacturing system. Addressing this substantial energy loss becomes essential for achieving a more energetically sustainable industrial application of the FSW/P process.

Declaration of competing interest

The authors declare that they have no known competing financial interests or personal relationships that could have appeared to influence the work reported in this paper.

Acknowledgments

PLI would like to acknowledge Fundação para a Ciência e a Tecnologia (FCT-MCTES) for its financial support via the PhD scholarship FCT-SFRH/BD/146885/2019. TGS, JPO and FF acknowledge Project 24534 - “INFANTE - Microssatélite para Vigilância Marítima, Observação da Terra e IoT no contexto de constelações”, supported by Operational Program for Competitiveness and Internationalization (COMPETE 2020) and Lisbon Regional Operational Programme (Lisboa 2020), under the PORTUGAL 2020 Partnership Agreement, through the European Regional Development Fund (ERDF). PLI, JPO and TGS acknowledge Fundação para a Ciência e a Tecnologia (FCT - MCTES) for its financial support via the project UIDB/00667/2020 and UIDP/00667/2020 (UNIDEMI). JPO acknowledges the funding of CENIMAT/i3N by national funds through the FCT-Fundação para a Ciência e a Tecnologia, I. P., within the scope of Multiannual Financing of R&D Units, reference UIDB/50025/2020-2023.

References

[1] Forsström A, Bossuyt S, Yagodzinskyy Y, Tsuzaki K, Hänninen H. Strain localization in copper canister FSW welds for spent nuclear fuel disposal. J Nucl Mater 2019;523:347–59. https://doi.org/10.1016/j.jnucmat.2019.06.024.
[2] Savolainen K, Saukkonen T, Hänninen H. Localization of plastic deformation in copper canisters for spent nuclear fuel. World J Nucl Sci Technol 2012;02:16–22. https://doi.org/10.4236/wjnst.2012.21003.
[3] Santos TG, Lopes N, MacHado M, Vilaça P, Miranda RM. Surface reinforcement of AA5083-H111 by friction stir processing assisted by electrical current. J Mater Process Technol 2015;216:375–80. https://doi.org/10.1016/j.jmatprotec.2014.10.005.
[4] Hamilton C, Dymek S, Sommers A. A thermal model of friction stir welding in aluminum alloys. Int J Mach Tools Manuf 2008;48:1120–30. https://doi.org/10.1016/j.ijmachtools.2008.02.001.
[5] Yaduwanshi DK, Bag S, Pal S. Heat transfer analyses in friction stir welding of aluminium alloy. Proc Inst Mech Eng Part B J Eng Manuf 2015;229:1722–33. https://doi.org/10.1177/0954405414539297.
[6] Mishra RS, Ma ZY. Friction stir welding and processing. Mater Sci Eng R Rep 2005:50. https://doi.org/10.1016/j.mser.2005.07.001.
[7] Vilaça P, Quintino L, dos Santos JF, Zettler R, Sheikhi S. Quality assessment of friction stir welding joints via an analytical thermal model, iSTIR. Mater Sci Eng A 2007;445–446:501–8. https://doi.org/10.1016/j.msea.2006.09.091.
[8] Hattel JH, Sonne MR, Tutum CC. Modelling residual stresses in friction stir welding of Al alloys—a review of possibilities and future trends. Int J Adv Manuf Technol 2015;76:1793–805. https://doi.org/10.1007/s00170-014-6394-2.
[9] Li H, Gao J, Li Q, Galloway A, Toumpis A. Effect of friction stir welding tool design on welding thermal efficiency. Sci Technol Weld Join 2019;24:156–62. https://doi.org/10.1080/13621718.2018.1495868.
[10] Su H, Wu CS, Pittner A, Rethmeier M. Thermal energy generation and distribution in friction stir welding of aluminum alloys. Energy 2014;77:720–31. https://doi.org/10.1016/j.energy.2014.09.045.
[11] Meyghani B, Awang M. Welding Simulations Using ABAQUS: A Practical Guide for Engineers. 2022. p. 123.
[12] Meyghani B, Awang M. Developing a finite element model for thermal analysis of friction stir welding (FSW) using hyperworks. Lect Notes Mech Eng 2020:619–28. https://doi.org/10.1007/978-981-13-8297-0_64.
[13] Meyghani B, Wu C. Progress in thermomechanical analysis of friction stir welding. Chin J Mech Eng (English Ed) 2020:33. https://doi.org/10.1186/s10033-020-0434-7.
[14] Meyghani B, Awang M. The influence of the tool tilt angle on the heat generation and the material behavior in friction stir welding (FSW). Metals (Basel) 2022:12. https://doi.org/10.3390/met12111837.
[15] Meyghani B, Awang MB, Emamian SS, Mohd Nor MKB, Pedapati SR. A comparison of different finite element methods in the thermal analysis of friction stir welding (FSW). Metals (Basel) 2017:7. https://doi.org/10.3390/met7100450.
[16] Meyghani B. A modified friction model and its application in finite-element analysis of friction stir welding process. J Manuf Process 2021;72:29–47. https://doi.org/10.1016/j.jmapro.2021.10.008.
[17] Cavaliere P, Santis A, Panella F, Squillace A. Thermoelasticity and CCD analysis of crack propagation in AA6082 friction stir welded joints. Int J Fatigue 2009;31:385–92. https://doi.org/10.1016/j.ijfatigue.2008.07.016.
[18] Tasić P, Hajro I, Hodžić D. Simplification possibilities for estimation of FSW process efficiency by FEA. In: 17th Int. Res. Conf. Trends Dev. Mach. Assoc. Technol. TMT 2013, Istanbul, Turkey; 10-11 Sept. 2013 Simpl., 2013. p. 10–1.
[19] Vilaça P, Quintino L, Dos Santos JF. ISTIR - analytical thermal model for friction stir welding. J Mater Process Technol 2005;169:452–65. https://doi.org/10.1016/j.jmatprotec.2004.12.016.
[20] Upadhyay P, Reynolds AP. Effects of forge axis force and backing plate thermal diffusivity on FSW of AA6056. Mater Sci Eng A 2012;558:394–402. https://doi.org/10.1016/j.msea.2012.08.018.
[21] Upadhyay P, Reynolds A. Effect of backing plate thermal property on friction stir welding of 25-mm-thick AA6061. Metall Mater Trans A 2014;45:2091–100. https://doi.org/10.1007/s11661-013-2121-0.
[22] Lambiase F, Paoletti A, Di Ilio A. Forces and temperature variation during friction stir welding of aluminum alloy AA6082-T6. Int J Adv Manuf Technol 2018;99:337–46. https://doi.org/10.1007/s00170-018-2524-6.
[23] Baragetti S, Božić Ž, Arcieri EV. Stress and fracture surface analysis of uncoated and coated 7075-T6 specimens under the rotating bending fatigue loading. Eng Fail Anal 2020;112:104512. https://doi.org/10.1016/J.ENGFAILANAL.2020.104512.

[24] Radisavljevic I, Zivkovic A, Radovic N, Grabulov V. Influence of FSW parameters on formation quality and mechanical properties of Al 2024-T351 butt welded joints. Trans Nonferrous Met Soc China (English Ed) 2013;23:3525–39. https://doi.org/10.1016/S1003-6326(13)62897-6.
[25] Choi WJ, Morrow JD, Pfefferkorn FE, Zinn MR. Welding parameter maps to help select power and energy consumption of friction stir welding. J Manuf Process 2018;33:35–42. https://doi.org/10.1016/j.jmapro.2018.04.017.
[26] Ahn SH, Lee CM. A study on large-area laser processing analysis in consideration of the moving heat source. Int J Precis Eng Manuf 2011;12:285–92. https://doi.org/10.1007/s12541-011-0038-3.
[27] Salloomi KN, Al-Sumaidae S. Numerical validation of temperature distribution in friction stir welded aluminum 7075-T651 plates using pseudo heat transfer model. Ann Chim Sci Des Mater 2017;41:29–38. https://doi.org/10.3166/ACSM.41.29-38.
[28] Sutherland John W. Linke DAD and BS. Energy Efficient Manufacturing: Theory and Applications. Wiley. 2018.
[29] Shrivastava A, Krones M, Pfefferkorn FE. Comparison of energy consumption and environmental impact of friction stir welding and gas metal arc welding for aluminum. CIRP J Manuf Sci Technol 2015;9:159–68. https://doi.org/10.1016/J.CIRPJ.2014.10.001.
[30] Reza-E-Rabby M, Reynolds AP. Some effects of tool geometric features on friction stir weld response parameters. Sci Technol Weld Join 2018;23:575–84. https://doi.org/10.1080/13621718.2018.1430009.